Nanoregions of rocksalt AgI in AgBr microcrystals

A. P. Marchetti, J. C. Hansen,* S. Chen, M. Irving, R. Baetzold, and B. R. Sever
Imaging Materials and Media, R&D, Eastman Kodak Company, Rochester, New York 14650-1735, USA
(Received 25 October 2002; revised manuscript received 16 July 2003; published 11 March 2004)

Rapid addition of iodide causes the optically excited low-temperature donor acceptor luminescence from $AgBr_{1-x}I_x$ ($x<0.4$) microcrystals to shift to ≈580 nm whereas this luminescence is observed from 530 to 540 nm in microcrystals with homogeneous iodide incorporation. The band-gap energy in rapid iodide addition microcrystals is ≈0.1 eV smaller than the measured band-gap energy for iodide concentrations near the maximum solubility (≈40%) even when the total iodide content is only a few percent. Low-temperature photoluminescence and excitation spectroscopy, transmission electron microscopy (TEM) and computational methods have been applied to determine the structure responsible for this behavior. The data generated indicated that nanoregions of fcc rocksalt $AgBr_{1-x}I_x$ ($x>0.9$) are integrated into these microcrystals. These nanoregions of high iodide are strained and can engender the characteristic dislocations observed in the TEMs. Some dislocation features are removed by annealing (200 °C). Heating also causes the luminescence and band-gap energy to return to the values characteristic of the crystals with a homogeneous distribution of iodide.

DOI: 10.1103/PhysRevB.69.094107 PACS number(s): 78.55.Hx, 71.15.−m, 73.22.−f, 68.37.Lp

I. INTRODUCTION

AgBr/I microcrystals are widely used in many photographic products. At present most color negative films contain AgBr microcrystals with some sort of iodide phase, either from a homogeneous (slow) addition of iodide or from a rapid iodide addition (RIA) step in their fabrication.[1] The homogeneous AgBr/I system forms an amalgamation semiconductor up to the solubility limit at about 40% iodide.[2,3] The low-temperature optical absorption and luminescence spectra and ESCA data indicate that the valence band is shifted up in energy as the iodide level is increased.[3–5] The low-temperature photoluminescence (LTPL) from samples with a homogeneous iodide distribution was found to peak between 525 and 540 nm depending on the iodide concentration. It has been shown that RIA microcrystals have a LTPL luminescence band at ≈580 nm that is characteristic of this manner of iodide addition.[6] The LTPL from RIA microcrystals appears to be due to some feature other than levels of iodide below the solubility limit.[3] In addition, experimental band-gap energies from melt grown samples up to $AgBr_{0.75}I_{0.25}$ were larger by ≈0.1 eV than those measured in RIA microcrystals (see below). Recent work has also suggested that this LTPL feature might be due to a disordered phase.[7]

It is the purpose of this article to present evidence that indicates that the species responsible for this LTPL characteristic observed in RIA microcrystals are metastable nanoregions of δ-AgI, that is the high pressure fcc (rocksalt) phase. Data will suggest that these regions trap holes and that the inclusion of these nanoregions of δ-AgI contributes to the formation of some types of dislocations that are observed in transmission electron microscopy (TEM) of RIA microcrystals.

II. EXPERIMENT

The samples used in this investigation were dispersions of AgBr/I microcrystals in gelatin. These AgBr/I microcrystal dispersions were fabricated by a double jet addition of solutions of $AgNO_3$ and NaBr(KI) to a stirred reaction vessel containing gelatin at temperatures between 50 and 70 °C.[8] Bromide ion concentration is used to control the microcrystal morphology. Low bromide ion concentrations (10^{-4} molar) favor cubic morphologies with (100) bounded surfaces, whereas higher bromide ion concentrations (10^{-2} molar) favor octahedral morphologies with (111) bounded surfaces. Nucleation at somewhat higher bromide ion concentrations (4×10^{-2} molar) causes the formation of parallel twin planes that engender a tabular morphology with (111) surfaces.

Regions with homogeneous levels of iodide were created in microcrystals by precipitation with mixed bromide and iodide solutions. The concentrations of iodide ranged from 1% to more than 25%. Iodide concentrations were calculated from the stoichiometry. Total iodide levels have been confirmed in a number of samples by neutron activation analysis.

The RIA microcrystals were created by adding, at some point during the precipitation of AgBr (or AgBr/I) microcrystals, a dispersion of AgI nanocrystals or adding rapidly a solution of KI and continuing the precipitation using $AgNO_3$ and NaBr solutions.[9] Samples were taken from the fabrication reactor just after the rapid KI addition to confirm spectroscopically the presence of AgI. When added rapidly, the amount of iodide constitutes only a few percent of the total halide. Although band-gap energies were obtained from a large number of samples, both microcrystals and melt grown crystals, only two examples are detailed below. Both are 1.5×0.1 μm* (* equivalent circular diameter×thickness) $AgBr_{0.97}I_{0.03}$ tabular microcrystal dispersions. The first is a homogeneous iodide microcrystal dispersion that has a local iodide concentration of 6 mol % initiated after 20% of the silver was added and continued for 50% of the fabrication. The second is a RIA microcrystal dispersion with a 3% rapid AgI addition at 70% of the silver addition.

The LTPL measurement apparatus has been described previously.[10] Samples of the microcrystal dispersions were

placed in a dewar and the temperature lowered to 6 K. The samples were excited by gas laser lines (325 or 442 nm) or from a xenon lamp and monochromator. The luminescence was focused on the slits of a 3/4 meter scanning monochromator. Excitation spectra were obtained by monitoring the luminescence intensity and scanning the excitation wavelength. The luminescence spectra were corrected for the monochromator-photomultiplier response and the excitation spectra were corrected for lamp-excitation monochromator output. Luminescence decay measurements were made on samples using a tripled Nd/YAG pulsed laser and a digitizer. Before annealing, the gel was removed from the microcrystals by several cycles of washing with distilled water and centrifugation. The microcrystals were placed in a furnace at temperature for one hour.

The data on the band-gap energies of the $AgBr_{1-x}I_x$ melt grown crystals were taken from Ref. 3. The method of obtaining the band-gap energy from excitation spectra is straightforward. In the weak absorption region, the luminescence intensity is proportional to the extinction coefficient for a given intensity of exciting light. The square root of the excitation intensity around the band edge is plotted vs the excitation energy.[11] The linear portion of this plot is extrapolated to zero intensity and this intersection provides the indirect edge band-gap energy. Even if only a portion (10 to 50%) of the AgBr microcrystal contains a homogeneous level of iodide, most of the radiative recombination at low temperature takes place in this region because the valence band has been shifted upwards and the region acts as a quantum well.[5] Thus the band-gap energies that are determined are for the region with the smallest gap.

Microcrystal dispersions with known homogeneous levels of iodide along with several different melt grown samples were used to check the excitation method for obtaining band-gap energies. The uncertainty in the direct absorption measurements was thought to be ± 5 meV, while the measurements from the excitation spectra was ± 10 meV.

Room temperature band-gap energies were obtained on some microcrystal dispersions by measuring their diffuse reflectance spectra and transforming this data with the Kubelka-Munk relation to derive data proportional to the optical density. The reflectance spectra were obtained using a 0.32 m grating spectrograph with a CCD detector. A 100 W quartz-halogen lamp provides excitation in the near infrared and visible. To avoid the effects of stray light, a diffuse illumination and specular detection mode is used. The raw reflectance data were transformed using the Kubelka-Munk equation to K/S data. The Kubelka-Munk equation is $K/S = (1-R_{\mathrm{inf}})^2/2R_{\mathrm{inf}}$, where R_{inf} is the measured reflectance of a sample of sufficient thickness, such that no light penetrates completely through the sample. This condition is satisfied as the samples are high scattering and flow through a 1-mm-thick flow cell. The absorption coefficient, K, bears the same significance as that customarily employed in spectroscopy by transmission techniques.[12] The scattering coefficient, S, is not easily identified. However, for the samples studied here, the contribution from scattering should not change significantly between samples based on the equivalent baselines observed for wavelengths greater than 550 nm. Thus, the conversion to K/S data relates the reflectance signal to the concentration of the absorbing species. Further analysis of the data yielded plots of the square root of the K/S data vs energy. This permits the derivation of band gap by calculation of the intercept of the initial slope with the baseline.

Transmission electron microscopy analysis of $AgBr_{1-x}I_x$ tabular microcrystals were carried out using a double-tilt sample holder (Gatan 636-DH), with the sample cooled by liquid nitrogen, and the microscope operating under 200 kV accelerating voltage. Annealing experiments were carried out with the crystals spread on carbon film deposited on Ta grids, inside the TEM under a vacuum of $\sim 10^{-8}$ torr, using a TEM heating holder (Gatan 628). Suitable AgX cross sections were cut using a diamond cryoknife in a Reichert Ultra-Cut S, and sections were picked up with a drop of 3 molar sucrose solution. Analytical electron microscopy (AEM) analysis used a focus electron beam with a diameter of ~ 20 nm, and composition analysis were calculated based on the Cliff-Lorimer equation, using AgBr and AgI as references.

The band-gap energy for face centered cubic (fcc) AgI has been determined as a function of pressure.[13] The room temperature value is 2.26 eV at the transition pressure of 7 kbar (0.7 GPa) with a lattice constant of 6.067 Å. The band gap energy decreases with increasing pressure and has a pressure dependence of -61 meV/GPa.

A. Computation

Atomistic modeling techniques have been used previously to study various bulk and surface structural properties of silver halide.[14,15] In the present work the stability of clusters of AgI within the bulk fcc AgBr crystal is studied. These calculations are based upon ionic models developed within the scope of the shell model that allows ions to polarize and permits the dielectric properties of the crystal to be represented.[16] In addition to the coulombic interactions, short-range interactions are treated with Buckingham type terms. This procedure has been developed and tested for AgCl and AgBr, where potentials that represent the structure, dielectric and elastic properties of the crystal have been developed.[17] These potentials also give good descriptions of the ionic defect formation energies in these crystals. A potential was not available for wurtzite AgI, so we followed

TABLE I. Buckingham and shell model parameters for AgI wurtzite potential.

(A) Buckingham terms, $V(r) = A\exp(-r/\rho) - C/r^6$

Interaction	A(eV)	ρ(Å)	C(eV Å^6)
Ag-I	5311.8	0.2979	142.6
I-I	46968.1	0.3097	100.0
Ag-Ag	16528.0	0.2310	224.0

B. Shell parameters

Ion	Shell charge (q)	K(q/Å^2)
Ag	-33.5906	7521.11
I	-4.087	39.95

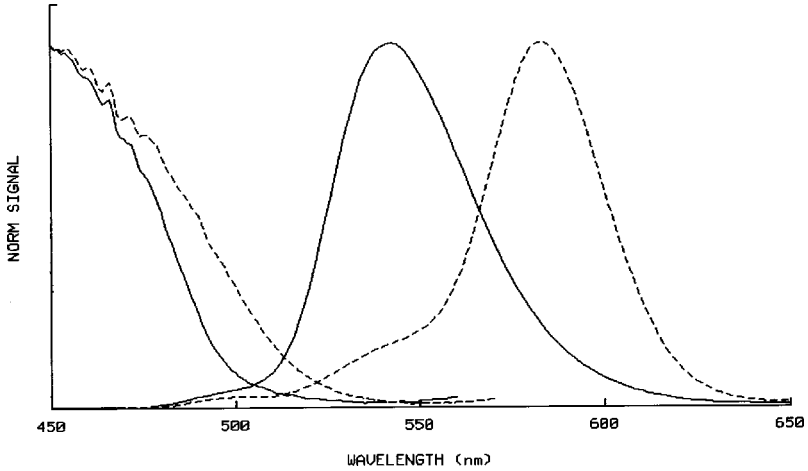

FIG. 1. The luminescence and excitation spectra of microcrystals with 6% homogeneous iodide over 50% of the microcrystal volume (solid line) and microcrystals with a 3% AgI addition at 70% of the growth (dashed line). For the luminescence spectra (right), the excitation wavelength was 325 nm. The excitation spectra (left) were obtained with monitoring wavelengths of 540 and 580 nm for the homogeneous and RIA microcrystals, respectively. The sample temperature was 6 K.

procedures similar to those used to develop AgCl and AgBr potentials in order to develop a working potential. We found it necessary to include three-body bond harmonic terms to the potential for Ag-I-I, I-Ag-Ag and Ag-Ag-Ag components as a means to include possible covalent interactions in this material. [These terms were obtained by fitting to the structure and elastic constants]. The parameters for the AgI wurtzite potential are given in Table I and the values for the AgBr potential are taken from Ref. 17.

The general utilities lattice program (GULP) written by Gale is used to calculate the stability of AgI units within the AgBr crystal.[18] This code is based upon the Mott-Littleton procedure and we employ a region of 9.0 Å radius in which all ions are fully treated and surrounded by another spherical region of 22 Å radius in which ions are treated by the harmonic part of the potential. The rest of the crystal is treated by continuum methods. The AgI cluster is placed at the center of the crystal and substituted for various numbers of AgBr ions. A complete description of the method may be found in Ref. 18.

III. RESULTS AND DISCUSSION

Figure 1 compares the LTPL and excitation spectra obtained from dispersions of RIA and homogeneous iodide tabular microcrystals of composition $AgBr_{0.97}I_{0.03}$. The homogeneous iodide microcrystals exhibit a single luminescence band peaking at $\approx$540 nm. This band is due to donor acceptor (DA) recombination in the homogeneous bromoiodide phase. A small inflection at $\approx$500 nm is due to iodide bound exciton radiative recombination from traces of iodide in the region that is pure AgBr.[3] For the RIA microcrystals, the dominant luminescence band is observed at $\approx$580 nm. This is the signature of a RIA procedure and has been associated with a unique bromoiodide phase. A slight inflection at $\approx$540 nm is due to the presence of a small portion of the added iodide that is uniformly distributed, after the RIA step. Microcrystals of cubic and octahedral morphology fabricated with a RIA step also have a LTPL peaking at $\approx$580 nm.

The effects of annealing on luminescence from the RIA sample (same as those in Fig. 1) are shown in Fig. 2. Even after the lowest temperature annealing at 120 °C, much of the RIA related luminescence at 580 nm has shifted to 540 nm, indicating the unique defect character of the RIA region has been significantly modified. For the 120 and 160 °C treatments, the RIA luminescence remains observable at 580 nm, indicating that not all of the RIA ''defect'' character was changed. For the 200 °C treatment, only a slight extension on the long wavelength side of the homogeneous iodide luminescence band remains indicating that the RIA region is lost. The luminescence from RIA microcrystals after a 200 °C anneal for 1 h is characteristic of microcrystals with a homo-

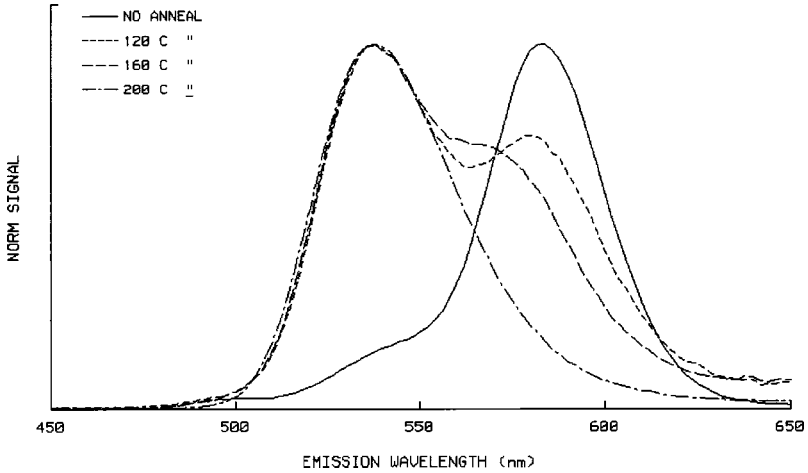

FIG. 2. The luminescence spectra from a RIA microcrystal dispersion after annealing at various temperatures for 1 h (no anneal: solid line; 120 °C: dotted line; 160 °C: dashed line; 200 °C: dot-dash line). The excitation wavelength was 325 nm and sample temperature was 6 K.

TABLE II. The band-gap energies in electron volts (eV) derived from the LT excitation spectra for the homogeneous and RIA tabular microcrystals untreated and annealed at 200 °C.

Monitoring wavelength	RIA (no anneal)	Homogeneous (no anneal)	RIA (200 °C)	Homogeneous (200 °C)
540 nm	2.50 ± 0.02	2.52	2.51	2.51
580 nm	2.34[a]	2.49	2.45	2.50

[a]The average band-gap energy for 9 different RIA samples was 2.35 ± 0.014 eV.

geneous level of iodide between 3 and 10%.

Only a slight shift of the luminescence band to shorter wavelengths is seen with increasing annealing temperature in the homogeneous iodide microcrystals. This shift in the luminescence peak to shorter wavelengths is suggestive of a subtle redistribution of the iodide into the iodide-free zones on either side of the iodide-containing zone.

Excitation measurements were taken on all samples. The luminescence was monitored in a range covering both the homogeneous and RIA iodide bands. Band-gap energies calculated from these measurements for the unannealed and 200 °C annealed samples are summarized in Table II. The unique LTPL associated with a RIA step and the decrease in the band-gap energy is suggestive of a new region that is also hole trapping like $AgBr_{1-x}I_x$ regions in AgBr.

For the microcrystals with only homogeneous bromoiodide zones, the band-gap energy is independent of monitoring wavelength and annealing. Note that the luminescence intensity is very weak at 580 nm in the homogeneous bromoiodide microcrystals. The RIA microcrystals before annealing exhibit a lower band-gap energy when monitoring the 580 nm luminescence. After annealing, the spectroscopic signature of the RIA region ''disappears'' and the band-gap energy is now that of a homogeneous iodide microcrystal independent of the monitoring wavelength. This change in the band-gap energy has implications for charged carrier processing within the microcrystals, particularly the hole trapping ability of the elevated iodide structures.

The luminescence decay after pulsed excitation has been characterized as DA recombination from plots of log intensity vs log time.[4] These luminescence decay plots of the annealed and unannealed homogeneous iodide microcrystals were almost identical, indicating that the recombination time behavior in these microcrystals is unchanged by annealing. The luminescence decay of the RIA microcrystals differs significantly from that of the homogeneous iodide samples. The decay behavior of the RIA microcrystals is changed upon annealing to closely resemble that of the homogeneous bromoiodide microcrystals.

Figure 3 shows a plot of the band-gap energies of $AgBr_{1-x}I_x$ as a function of iodide concentration (x) at both 4 and 300 K. The gap energy (2.35 ± 0.05 eV at 4 K) determined from the RIA luminescence by analyzing the excitation spectra were *arbitrarily* placed at $x = 0.9$ in Fig. 3. The band-gap energy for rocksalt δ-AgI at 4 K is estimated using the difference in band-gap energy at 4 and 300 K for the $AgBr_{1-x}I_x$ samples. The data shown in Fig. 3 indicate that the band-gap energies are a monotonically decreasing function of the mole fraction of iodide. These data also indicate that the value of the band-gap energy obtained from the RIA luminescence is suggestive of these regions being (rocksalt) δ-AgI.

Measured band-gap energies for the known forms of AgI and other fcc silver halides are shown in Table III.[19,20] A consideration of these energies and the data in Fig. 3 indicate that the best match for the species formed with a ''nonequilibrium'' addition of iodide (that is a RIA procedure) is δAgI or more realistically a $AgBr_{1-x}I_x$ region where x is close to 1. The only other possible specie might be αAgI, which should only be stable above 417 K. If this specie were to exist at low temperature, its band-gap energy could be estimated. Using the known temperature dependence of γAgI and the various $AgBr_{1-x}I_x$ samples, the band-gap energy of αAgI would be placed at about 2.55 eV at 4 K, which is inconsistent with the measured band-gap energies near 2.35 eV for the RIA materials.

Fabrication of microcrystals with homogeneous iodide regions can induce the formation of stacking faults defects with an $a/6[1\bar{2}1]$ displacement vector.[21,22] Under low magnification imaging condition in TEM, these defects are manifested as striation contrast bands running parallel to the microcrystal edges [Fig. 4(a)]. In RIA microcrystals, at least

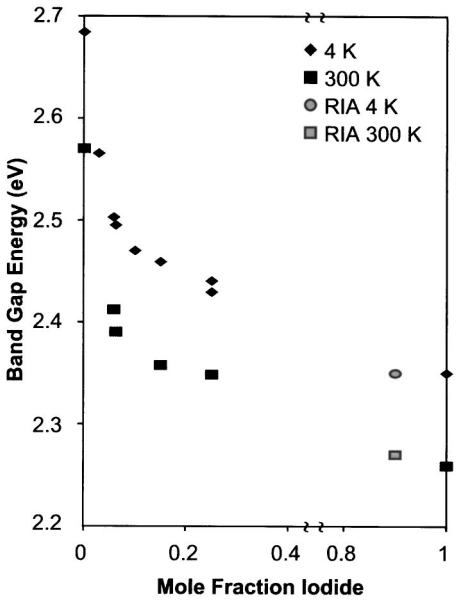

FIG. 3. The band-gap energies of a number of $AgBr_{1-x}I_x$ samples as a function of the mole fraction iodide, the high-pressure rocksalt δ-AgI (from literature) and the species found in RIA microcrystals are referenced at 1.0 and 0.9 mole fraction iodide, respectively. These data are given at 300 and 4 K.

TABLE III. Measured band-gap energies for various forms of AgI, $AgBr_{.75}I_{.25}$ and AgBr.

Temp(K)	αAgI(bcc)	βAgI(hcp)	γAgI(zb)	δAgI(fcc)	$AgBr_{0.75}I_{0..25}$	AgBr
4		3.023	2.91	$(2.35)_{est}$	2.44	2.71
300			2.82	2.26	2.34	2.57
>420	2.40 eV					

two other structural defects caused by the rapid addition of iodide have been documented. The first is coincident with the crystal growth point at which iodide is rapidly added, resulting in the formation of an edge-type dislocation, located within the crystal and positioned concentrically parallel to the microcrystal edges [Fig. 5(a)]. This line separates the region of iodide addition from the AgBr core. It exhibits diffraction contrast consistent with a defect core characterized with a Burgers vector value of $a/6[1\bar{2}1]$.[23] The second defect is a collection of short dislocation segments that starts from the rapid iodide addition dislocation line and extends a short distance through the AgBrI perimeter region out to the edge of the microcrystal. $(\bar{2}02)$ two-beam dark field image analyses indicates that these contain a core structure with mainly $a/2[\bar{1}01]$ characteristics.[21]

Annealing studies have provided additional insight into the relationships among these structural defects. Experimental details of sample preparation, TEM imaging, and annealing conditions have been described previously.[24] Annealing homogeneous iodide microcrystals in a TEM hot stage (at $\sim 10^{-8}$ torr) induced a gradual reduction of the stacking faults starting at $\sim 160\,^{\circ}$C, followed by their disappearance by $220\,^{\circ}$C. By $200\,^{\circ}$C, only the stacking fault marking the boundary between the pure AgBr core and the AgBr/I shell remained [Figs. 4(b) and 4(c)]. These annealing results are consistent with those reported previously.[24,25] By comparison, heating the RIA microcrystals to $\sim 160\,^{\circ}$C caused some reduction to the intensity of the $a/6[1\bar{2}1]$ dislocation lines, but the $200\,^{\circ}$C treatments completely annealed away this feature. However, no discernible effect on the $a/2[\bar{1}01]$ dislocation segments was observed [Figs. 5(b) and 5(c)].

Analytical electron microscopy (AEM) analysis, using a 20-nm diameter focused electron beam, was used to monitor iodide movement associated with annealing. The AEM technique is capable of measuring the composition of small areas. Local iodide content at various locations (A, B, C, D in Figs. 4 and 5) within individual microcrystals was probed. For homogeneous iodide crystals, the data indicated a slight increase (0.5 mol %) in iodide content in the pure AgBr region after annealing microcrystals with homogeneous bromoiodide regions [Fig. 4(d)]. However, this increase is within the experimental error of the technique and therefore cannot be taken as definitive. Similarly, in RIA microcrystals no significant iodide movement was detected [Fig. 5(d)]. In

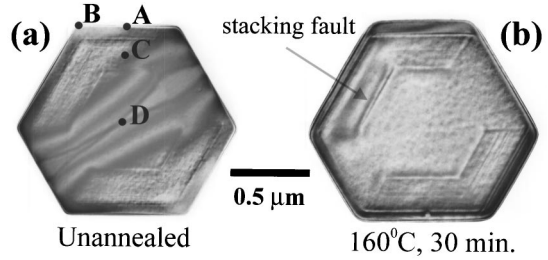

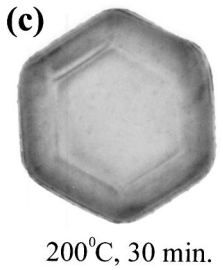

Local [I⁻] Analysis [±0.5%]

	25°	160°	200°
A	0 %	0	0.5
B	0	0	0.5
C	6	6	6
D	0.5	0.5	0.5

FIG. 4. Annealing study of microcrystals with homogeneous iodide regions. TEM images showed the striation contrast defects in these tabular crystals anneal away by $\sim 200\,^{\circ}$C. Note that the crystals in (a) and (b) were image under $(\bar{2}02)$ two-beam conditions, to provide zero contrast to one of three sets of $a/6[1\bar{2}1]$ stacking fault defects, and at the same time maximizing the contrast to the other two equivalent sets of stacking fault fringes.

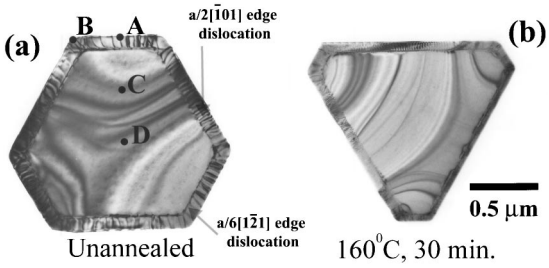

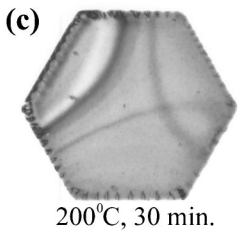

Local [I⁻] Analysis [±0.5%]

	25°	160°	200°
A	6 %	6	6
B	6	6	6
C	1	1	1
D	1	1	1

FIG. 5. Annealing study of RIA microcrystals. TEM images showed that only the $a/6[1\bar{2}1]$ dislocation defects in these platelet crystals anneal away by $\sim 200\,^{\circ}$C. It is pointed out that the width of the outer band between the crystal edge and the $a/6[1\bar{2}1]$ dislocation lines, marking the RIA step, can vary among crystals. The crystals shown in (a), (b), and (c) were selected for their wider bands in order to clearly show the morphologies of the two types of dislocations in this outer perimeter region.

addition, attempts to monitor the size of the high iodide region at the $a/6[1\bar{2}1]$ dislocation lines in RIA microcrystals did not consistently show any experimentally significant iodide variation (between points separated by ~ 50 nm). Considering the size of the electron beam, and various beam-solid interactions, this technique may not be sensitive enough to determine any short-range iodide movement smaller than ~ 40 nm.

The $a/6[1\bar{2}1]$ edge dislocation in RIA AgBrI was analyzed further because of its apparent correlation to the 580 nm luminescence band intensity in LTPL. From TEM results, it is possible to understand the location and the probable size of this feature. First, comparison to structural defects in the homogeneous iodide regions of $AgBr_{1-x}I_x$ microcrystals and their annealing characteristics at 200 °C is useful. Two similar defect structures in homogeneous $AgBr_{1-x}I_x$ are understood. Both not only show similar diffraction contrast characteristics, but also exhibit identical dislocation core structures. One is the stacking fault with the $a/6[1\bar{2}1]$ displacement vector that runs parallel to microcrystal edges [Fig. 4(a)].[21] Previous microscopy results have indicated that the stacking faults are located on the internal twin planes, and are manifested as small regions of multiply-twinned inclined planes.[22] The second is the dislocation network, which is manifested in TEMs under high magnification conditions as three sets of criss-crossing lines, rotated 120° from each other. From cross-section studies, these have been identified as being caused by a network of closely spaced jogs or steps on the internal twin planes.[24] Combined, these two defects impart a jagged morphology to the twin boundaries, when viewed edge-on in cross sections.[22] Two important similarities are noted. First, the $a/6[1\bar{2}1]$ edge dislocation in RIA microcrystals exhibits similar contrast characteristics to the two structural defects in homogeneous iodide AgBrI microcrystals. In fact, all three defects exhibit the same zero contrast property when imaged under the $(\bar{2}02)$ two-beam condition in the TEM. This suggests that the former is also a structural defect on the internal twin planes of RIA tabular microcrystals. This is further substantiated by the annealing results. The removal of the $a/6[1\bar{2}1]$ dislocations at ~ 200 °C in the RIA microcrystals, compares similarly to the loss of the multiple fringe contrast (from the stacking faults) and the gridlike contrast features in homogeneous iodide microcrystals when annealed,[24] and points to the similar core structure between these three defects in the AgBr/I lattice. Additional evidence on the location of these defects on the twin planes is the reported finding that accompanying the loss of striationlike fringes in homogeneous iodide microcrystals, is the transformation of the twin planes from a jagged to a smooth morphology after a 200 °C annealing treatment.[24] Hence, the $a/6[1\bar{2}1]$ dislocation feature in RIA microcrystals is likely located on the internal twin planes as a step or jog.

Direct evidence of the $a/6[1\bar{2}1]$ dislocation as a perturbation to the twin planes has been found in cross sections of RIA microcrystals. Under low magnification conditions, with electron beam carefully aligned along $[10\bar{1}]$, two distinct

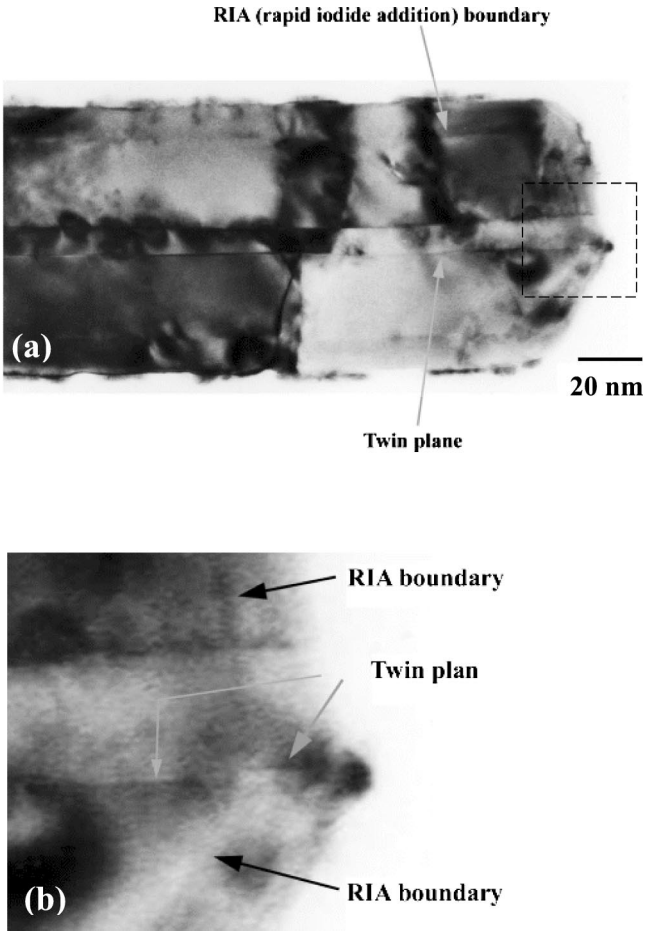

FIG. 6. (a) A TEM image of a cross-sectioned segment of a tabular RIA microcrystal, collected with the beam aligned in order to observe the (111) twin planes edge on. A lattice distortion region, coincident with the rapid incorporation of iodide is seen. This line is labeled as RIA boundary. It is pointed out that the process of microtoming AgBrI invariably introduce some sectioning artifacts, including folding and cracking of the crystal and platelets. This induces nonuniformity of contrast over relatively large regions of the cryosections. However, within each region of similar contrast, imaged details of structural features are interpretable. (b) Enlargement of the inset from (a) showing details of the intersection of the RIA boundary with the twin plane.

features have been found. First, a concentric, linear feature inside the tabular microcrystal is seen, labeled as ''RIA boundary'' [Fig. 6(a)]. AEM analysis on this line with a 20-nm diameter electron probe indicated a relatively high iodide concentration ranging from 12–18 mol %. For neighboring regions towards the platelet center, the iodide concentration, [I], was found to be 0%, while in the direction towards the surface, the [I] decreased gradually until it reached a value of 5–6 mol % iodide at the tabular microcrystal surface. While this data shows that the RIA boundary line correspond to a region of high [I], it does not have the spatial resolution to discriminate the actual [I] at the center/core of this line. However, it is likely that the core of the RIA boundary has a much higher [I] than the measured 12–18 mol % iodide, given the AEM measurement sampled the core and its surrounding matrix. It is even possible that the small core

is nearly pure AgI. High magnification and electron diffraction studies did not reveal another structural phase in the RIA boundary region. This suggests a high iodide phase isostructural with the face-centered-cubic AgBr lattice. By comparison, in cross-section microscopy studies of homogeneous iodide AgBrI microcrystals, no feature resembling the RIA boundary has been found,[24] suggesting that the fcc phase of saturated iodide AgBr/I is not at the core of the RIA boundary line. The morphology of this region suggests that TEM is imaging a strained field around the core, which is isostructural with the fcc AgBr matrix, yet its lattice constant is significantly different. One possible core structure would be the high-pressure phase form of AgI, which has a rocksalt lattice, with a lattice parameter that is $\sim 10\%$ larger than that of AgBr.

The second intriguing feature noted is at the intersection of the RIA boundary with the twin planes. It is noted that at this intersection a jog/step on the twin boundary occurs on at least one of the twin planes [Fig. 6(b)]. Hence, this jog is located in a region high in iodide. Prior dislocation analysis has proposed that an $a/6[1\bar{2}1]$ twinning dislocation on the twin boundary is an off-set across the twin plane by n/2 of the (111) spacing, where n is an odd integer. This step is charged and is expected to occur with an excess of halide across this step.[26] Therefore, this additional evidence also suggests that the core of such a jog is a nanoregion of pure AgI. This region is expected to be very small, $\sim$ two (111) layers thick, one on either side of the jog, or ~ 0.63 nm. The presence of such a small region AgI is consistent with the lack of diffraction or stoichiometric quantification as discussed earlier. The offset, caused by the $a/6[1\bar{2}1]$ twinning dislocation seen in these cross sections, correspond to the linear feature identified as the $a/6[1\bar{2}1]$ edge dislocation in plan-view images, Fig. 5(a). However, the related $a/2[\bar{1}01]$ short dislocation segments seen in plan views would extend from the jog on the twin boundary towards the outer edge of the crystal. Because these lie on the twin boundary, they are obscured by the contrast of this planar feature, and therefore, are not directly visible in cross-section images. The geometry of these two dislocations are consistent with that first proposed by Hamilton.[26]

The experimentally observed removal of this dislocation or jog on the twin boundary at 200 °C [Fig. 5(c)], coincident with the loss of the 580 nm LTPL luminescence, indicates a short-range movement of the atoms at the twinning dislocation. It is most likely that the change to the twin plane is the removal of the jog to form a straight twin plane boundary line, similar to what has been demonstrated for homogeneous iodide AgBrI.[24] This evidence of atomic rearrangements also points to the possibility that the small high iodide regions can relax and diffuse into the surrounding lattice in the RIA boundary line, thus removing the ''cause'' of the 580 nm luminescence. Finally, it should be noted that the existence of a high-pressure metastable phase within the lattice of another phase is known to exist in other materials.[27]

The question of the existence of a high-pressure phase can be discussed from several points of view. It is known that thin layers (below some critical thickness) of epitaxial deposits can be elastically strained resulting in a commensurate interface where the epitaxial phase adopts the crystal structure of the host substrate.[28] Thus it might be expected that very small regions of silver iodide might take the crystal structure of the host, that is, fcc (rocksalt) instead of the ambient temperature and pressure phases which are hcp (wurtzite) and fcc (zincblende). Further the lattice mismatch will cause an effective pressure on that region making a ''high pressure'' phase more likely. The pressure can be estimated from classical considerations using an attractive Madelung potential with an exponential repulsive term.[29] The potential is described by Eq. (1), where $A=(ze)^2\ \alpha'$, z is the ''valence,'' e is the charge on an electron, and α' is the Madelung constant,

$$u(r)=-A/r+Be^{-r/\rho}, \tag{1}$$

while B and ρ are determined constants. The pressure is the negative derivative of the potential with respect to the volume (v) as given by Eq. (2) with $p=0$ at $r=r_0$,

$$p=-du(r)/dv=1/3v\{-A/r+B(r/\rho)e^{-r/\rho}\}. \tag{2}$$

To estimate the pressure for a given lattice mismatch, the pressure expression can be expanded in Taylor Series about r_0 and keeping only the first term, yielding Eq. (3):

$$\begin{aligned} p(r)&=p(r_0)+p'(r_0)(r-r_0)\\ &=1/3v_0r_0\{2A/r_0-A/\rho\}(r-r_0). \end{aligned} \tag{3}$$

Substituting in the value for α' for a rocksalt fcc lattice and determining ρ from the compressibility[20] of AgBr gives an upper limit of $p=4.9\times10^8$ N/m^2 (Pa) $=4.9$ kbar for the example where one Br ($r=1.95$ Å) is replaced with one I ($r=2.16$ Å) and assuming that the AgBr lattice is not distorted. The calculated pressure is of the same order of magnitude as the phase transition pressure of 7 kbar needed to go to the fcc (rocksalt) phase of AgI. If a number of bromides in several nonprimative unit cells were replaced, the estimated upper limit to the pressure would increase. While this is a classical picture, the Madelung potential [(Eq. (1)] predicts lattice energies to better than 10% and Eq. (3) should give a reasonable estimate of the magnitude of the pressure (strain) in the lattice. A 10% lattice mismatch, as expected with rock salt forms of AgBr and AgI, is generally considered far in excess of the elastic limit and thought likely to generate dislocations rather than retain epitaxial lattice commensurability. However, such expectations are generally applied to two bulk materials when brought into contact. If such regions are small or thin, it is not uncommon for the expected strain energy per unit area to be accommodated by the elasticity in either the host or epitaxial material.[30] The formation of strained regions after a rapid addition iodide step with continued overgrowth of the parent material suggests a general mechanism for the formation of certain dislocations associated with RIA microcrystals.

Another way to look at the internal ''pressure'' is to consider the strain near an AgI cluster. The computational question is whether a small region of δAgI could be stable within the AgBr crystal. We first substituted AgI ion pairs for AgBr

in spherical arrays containing AgI_6, AgI_6Ag_{12} and then $AgI_6Ag_{12}I_8$. The system was allowed to relax to equilibrium resulting in a AgI cluster remaining in the ''rocksalt'' structure in all of these cases. The Ag-I bond length was elongated by up to 0.1 Å over the normal Ag-Br bond length of 2.864 Å. Next we considered cubic and rectangular clusters of ions including Ag_6I_6 ($3\times2\times2$), Ag_9I_9 ($3\times2\times3$), $Ag_{13}I_{14}$ ($3\times3\times3$), $Ag_{18}I_{18}$ ($4\times3\times3$), and $Ag_{37}I_{38}$ ($5\times5\times3$). In each case, the resulting relaxed structure remained fcc rocksalt with displacements from the original AgBr sites of up to about 0.15 Å. In the case of the largest cluster the Ag-I bond lengths were up to 0.15 Å greater than AgBr, but the displacement off cubic sites was less than 0.01 Å. Therefore, in no case did we observe a change to wurtzite structure even though the AgI potential is that for a wurtzite crystal structure.

Subsequently, we considered substituting wurtzite units of AgI within the AgBr crystal. We substituted tetrahedral AgI_4 for $AgBr_6$. This structure relaxed back to nearly the octahedral sites of the rocksalt structure. Of course, a perfect octahedral structure would not be expected because of the presence of two vacancies. Next, we considered a larger $Ag_{13}I_{14}$ cluster in the wurtzite structure substituted for various sized AgBr clusters in order to provide sufficient space for the AgI cluster. In all of these cases the lattice was unstable. Thus, the computations were not able to find a stable wurtzite structure of AgI within the fcc AgBr. These computations indicate that small regions of fcc rocksalt δAgI are stable in an AgBr lattice.

The existence of nanoregions of AgI in AgBr/I raises the possibility of quantum confinement effects further influencing the spectroscopic data.[31] Quantum size effects occur when there is a ''confining'' potential, such as a semiconductor-vacuum interface and where there is a sizable discontinuity in the dielectric constant. The confining potential is small, 0.1 to 0.3 eV, the difference in valence band energy in $AgBr_{1-x}I_x$ or AgBr and δAgI. The hole binding energy will depend on the size of the region, but is likely to be on the order of 100 meV or less. The change in dielectric constant going from an AgBr region to a region that is nearly pure AgI should be relatively small. Based on the difference in dielectric constant[20] in AgCl (9.55) and AgBr (10.64), the δAgI dielectric constant is estimated to be about 11.5. With the small binding energy and the small difference in dielectric constant it would be expected that practically, there is little or no quantum confinement.

IV. CONCLUSIONS

This investigation has detailed the experimental and theoretical observations pertaining to the structure created when iodide, either as a KI solution or as AgI nanocrystals, is added rapidly during the aqueous precipitation of AgBr microcrystals with a gelatin peptizer. LTPL has identified an luminescence ''specie'' specific to AgBr(I) microcrystals that results from a RIA procedure. Extrapolations of measured band-gap energies strongly suggest that the luminescence specie or species are related to small regions of a nearly pure δAgI phase-specifically fcc rocksalt AgI. Simple assumptions using Madelung potential energy calculations suggest that small regions of δAgI confined within a AgBr lattice result in localized pressures comparable to the formation pressures required for formation of bulk rocksalt AgI. Computations indicate that small regions of fcc rocksalt AgI are stable in an fcc AgBr lattice structure. Computations further indicate that small regions of hcp (wurtzite) AgI in a rocksalt AgBr lattice are unstable.

Detailed microstructure analysis by TEM suggests the likely presence of a high iodide region inside the AgBrI crystal, coinciding with the introduction of AgI (or KI) during the crystal preparation process. Structural analysis of the dislocations induced by the rapid addition of iodide points to the presence of a high iodide rocksalt structure at its core. It is likely centered in the RIA region. This RIA region is the source of the 580 nm LTPL in AgBr/I microcrystals. In tabular microcrystals, the intersection between the RIA boundary and the internal twin planes generates a jog/step on the twin plane that has been observed. Such structural elements are suggestive of the size of such a core region, and may only be ~two (111) layers thick, or ~0.6 nm. Annealing to 200 °C removes the $a/6[1\bar{2}1]$ dislocation, coincidence with the disappearance of the 580 nm LTLP band. This suggests short-range atomic movement can occur to ''dilute'' the AgI core to blend into its isostructural AgBrI matrix.

The high iodide structure detailed above in RIA AgBr/I microcrystals appears to be related to the high efficency built into most color negative photographic films.

ACKNOWLEDGMENTS

The authors would like to thank Joe Hodes for technical support and A. E. Taddei for assistance with preparing cryosections, and collecting some of the electron microscopy data. We would like to thank Ralph Young for helpful and interesting discussions.

*Author to whom correspondence should be addressed. Email address: jeffrey.hansen@kodak.com

[1] J. Solberg *et al.*, U.S. Patent 4,433.048 (1984); H. Wilgus *et al.*, U.S. Patent 4,434.226 (1984); R. Piggin *et al.*, U.S. Patent 5,061,609 (1991) and U.S. Patent 5,061,616 (1991).

[2] O. Stasiw and J. Teltow, Z. Anorg. Chem. **249**, 143 (1949).

[3] A. P. Marchetti and M. S. Burberry, Phys. Rev. B **37**, 10 862 (1988).

[4] A. P. Marchetti and M. S. Burberry, Phys. Rev. B **28**, 3130 (1983).

[5] M. G. Mason, Y. T. Tan, T. J. Miller, G. N. Kwawer, F. C. Brown, and A. B. Kunz, Phys. Rev. B **42**, 2996 (1990).

[6] E. Chang *et al.*, U.S. Patent 5,314,793 (1994) and U.S. Patent 5,360,703 (1994); X. Wen, U.S. Patent 5,470,698 (1995); S. H. Ehrlich, J. Imaging Sci. Technol. **37**, 73 (1993).

[7] M. E. Irving, Proceedings of the International Congress on Imaging Science, Vol. 1, Extended abstracts, 1998.

[8] C. R. Berry, in *The Theory of the Photographic Process*, edited by T. H. James (Macmillan, New York, 1977), Chap. 3; U.S. Patent Number 5,147,771, Sept. 15, 1992; U.S. Patent Number 5,210,013, May 11, 1993.

[9] M. Irving *et al.*, US patent 5,728,515 (1998).

[10] A. P. Marchetti, P. J. Rodney, and W. von der Osten, Phys. Rev. B **64**, 132201 (2001).
[11] J. I. Pankove, *Optical Processes in Semiconductors* (Dover, New York, 1971), Chap. 3.
[12] W. Wendlandt and H. Hecht, *Reflectance Spectroscopy* (Wiley Interscience, New York, 1966), Chap. 3.
[13] S. Ves, D. Glotzel, M. Cardona, and H. Overhof, Phys. Rev. B **24**, 3073 (1981).
[14] R. C. Baetzold, J. Phys. Chem. Solids **57**, 627 (1996).
[15] R. C. Baetzold, Phys. Rev. B **52**, 11 424 (1995).
[16] B. G. Dick and A. W. Overhauser, Phys. Rev. **112**, 90 (1958).
[17] C. R. A. Catlow, J. Corish, J. H. Harding, and P. W. M. Jacobs, Philos. Mag. A **55**, 481 (1987).
[18] J. D. Gale, J. Chem. Soc., Faraday Trans. **93**, 69 (1997).
[19] *Semiconductors other than Group IV and III–V Compounds*, edited by O. Madelung (Springer-Verlag, Berlin, 1992).
[20] W. von der Osten, in *I–VII Compounds, Landolt-Börnstein, New Series Vol. 17b* (Springer-Verlag, Berlin, 1982), pp. 273–296.
[21] C. Goessens, D. Schryvers, J. Van Landuyt, S. Amelinckx, A. Verbeeck, and R. De Keyzer, J. Cryst. Growth **110**, 930 (1991).
[22] S. Jagannathan, S. Chen, R. V. Mehta, and R. Jagannathan, Phys. Rev. B **53**, 9 (1996).
[23] W. Van Renterghem, S. Karthauser, D. Schryvers, J. Van Landuyt, R. De Keyzer, and C. Van Roost, Proceedings of International Symposium on Silver Halide Imaging, 2000, Quebec, p. 167.
[24] S. Chen, A. E. Taddei, S. Jagannathan, and M. G. Antoniades, J. Imaging Sci. Technol. **45**, 230 (2001).
[25] C. Goessens, D. Schryvers, J. Van Landuyt, I. Geuens, R. Gijbels, W. Jacob, and R. De Keyzer, J. Imaging Sci. Technol. **39**, 70 (1995).
[26] J. F. Hamilton, Philos. Mag. **16**, 1 (1967).
[27] T. Y. Tan and H. Föll, Philos. Mag. A **44**, 127 (1981).
[28] A. P. Sutton and R. W. Balluffi, *Interfaces in Crystalline Materials* (Oxford University Press, New York, 1996), p. 108.
[29] M. Born and K. Huang, *Dynamical Theory of Crystal Lattices* (Oxford University Press, London, 1966), p. 24 ff.
[30] G. Burns, *Solid State Physics* (Academic, San Diego, 1990), p. 725.
[31] A. P. Marchetti and M. E. Freedhof, in *Semiconductor Nanocrystals, Handbook of Optical Properties Vol. II*, edited by R. E. Hummel and P. Wissmann (CRC, New York, 1997).